bioRxiv preprint doi: https://doi.org/10.1101/2020.05.18.102558; this version posted May 20, 2020. The copyright holder for this preprint (which was not certified by peer review) is the author/funder. All rights reserved. No reuse allowed without permission.

Practical gradient non-linearity correction of multi-site diffusion weighted MRI with empirical field maps

Colin B. Hansen*[1], Baxter P. Rogers*[2,3], Kurt G. Schilling[2], Vishwesh Nath[1], Justin A. Blaber[4], Okan Irfanoglu[5], Alan Barnett[5], Carlo Pierpaoli[5], Adam W. Anderson[2,3], Bennett A. Landman[1,2,3,4]

[1]Computer Science, Vanderbilt University, Nashville, TN, USA;
[2]Department of Radiology and Radiological Sciences, Vanderbilt University Medical Center, Nashville, TN USA;
[3]Department of Biomedical Engineering, Vanderbilt University, Nashville, TN USA;
[4]Electrical Engineering, Vanderbilt University, Nashville, TN, USA;
[5]National Institute of Biomedical Imaging and Bioengineering, Bethesda MD USA;

Corresponding Author:
Colin Hansen
PhD Student
Computer Science, Vanderbilt University
Email: colin.b.hansen@vanderbilt.edu

ACKNOWLEDGEMENTS

This work was supported by the National Institutes of Health under award numbers R01EB017230, and T32EB001628, and in part by the National Center for Research Resources, Grant UL1 RR024975-01. The content is solely the responsibility of the authors and does not necessarily represent the official views of the NIH.

bioRxiv preprint doi: https://doi.org/10.1101/2020.05.18.102558; this version posted May 20, 2020. The copyright holder for this preprint (which was not certified by peer review) is the author/funder. All rights reserved. No reuse allowed without permission.

ABSTRACT

Background: Achieving inter-site / inter-scanner reproducibility of diffusion weighted magnetic resonance imaging (DW-MRI) metrics has been challenging given differences in acquisition protocols, analysis models, and hardware factors.

Purpose: Gradient fields impart scanner-dependent spatial variations in the applied diffusion weighting that can be corrected if the gradient non-linearities are known. However, retrieving manufacturer non-linearity specifications is not well supported and may introduce errors in interpretation of units or coordinate systems. We propose an empirical approach to mapping the gradient nonlinearities with sequences that are supported across the major scanner vendors.

Study Type: Prospective observational study

Subjects: Two diffusion phantoms (High Precision Devices diffusion phantom and a custom isotropic phantom), five human control volunteers

Field Strength/Sequence: 3T (three scanners). Stejskal-Tanner spin echo sequence with b-values of 1000, 2000 s/mm^2 with 12 and 32 diffusion gradient directions per shell.

Assessment: We compare the proposed correction with the prior approach using manufacturer specifications against typical diffusion pre-processing pipelines (i.e., ignoring spatial gradient non-linearities). In phantom data, we evaluate metrics against the ground truth. In human and phantom data, we evaluate reproducibility across scans, sessions, and hardware.

bioRxiv preprint doi: https://doi.org/10.1101/2020.05.18.102558; this version posted May 20, 2020. The copyright holder for this preprint (which was not certified by peer review) is the author/funder. All rights reserved. No reuse allowed without permission.

Statistical Tests: Wilcoxon rank-sum test between uncorrected and corrected data.

Results: In phantom data, our correction method reduces variation in metrics across sessions over uncorrected data ($p<0.05$). In human data, we show that this method can also reduce variation in mean diffusivity across scanners ($p<0.05$).

Conclusion: Our method is relatively simple, fast, and can be applied retroactively. We advocate incorporating voxel-specific b-value and b-vector maps should be incorporated in DW-MRI harmonization preprocessing pipelines to improve quantitative accuracy of measured diffusion parameters.

Keywords: Gradient Non-linearity, Field Estimation, Pre-processing, DW-MRI

bioRxiv preprint doi: https://doi.org/10.1101/2020.05.18.102558; this version posted May 20, 2020. The copyright holder for this preprint (which was not certified by peer review) is the author/funder. All rights reserved. No reuse allowed without permission.

INTRODUCTION

Physical constraints of gradient coil designs result in a nonuniform magnetic field gradients during acquisition. This leads to spatial image warping [1-4] in magnetic resonance images and gradient distortion in diffusion weighted magnetic resonance imaging (DW-MRI) [5-9]. The introduced spatial variation can impact estimated diffusion tensor information [10] or high-angular resolution diffusion measurements [11]. Bammer et al. show in extreme cases the gradient nonuniformity can lead to an overestimation in the diffusion coefficient up to 30% and an underestimation up to 15% [12]. The effect's severity increases with distance from the magnet's isocenter [12] and with higher gradient amplitudes [12, 13]. The artifact becomes especially troubling for multi-site studies that have varying scanner models and manufacturers [14] and for studies utilizing very large gradient amplitudes such as in the human connectome project (HCP) which utilized amplitudes up to 300 mT/m [13, 15, 16]. Recent work has shown the effect of gradient nonlinearities in the HCP cohort results in considerable bias in tractography results and potentially incorrect interpretations in group-wise studies [17].

Various estimates of the coil field nonlinearities have been applied to improve accuracy within and across sites [18-21]. An adaptive correction of diffusion information proposed by Bammer et al. relies on calculating the spatially varying gradient coil L. This approach is achieved by relating the actual gradients with the desired gradients [12], and has become standard practice [22, 23]. However, this approach assumes that the gradient calibration specified by the manufacturer is readily available. Spherical harmonics (SH) based techniques are already implemented by manufacturers in the scanning systems to account for the spatial image warping effects of gradient

bioRxiv preprint doi: https://doi.org/10.1101/2020.05.18.102558; this version posted May 20, 2020. The copyright holder for this preprint (which was not certified by peer review) is the author/funder. All rights reserved. No reuse allowed without permission.

nonlinearities [1, 24-26]. Yet the SH coefficients are not usually provided to regular users and may be subject to non-disclosure criteria.

To remove the need for the manufacturer supplied specifications, we demonstrate an empirical field-mapping procedure which can be universally applied across platform as defined by Rogers et al. [27, 28]. At two scanner (scanner A and scanner B), a large oil-filled phantom is used to measure the magnetic field produced by each gradient coil. To estimate the achieved diffusion gradient directions and b-values on a voxel-wise basis, solid harmonic basis functions are fit to the measured magnetic field. The measured diffusivity (MD) and fractional anisotropy (FA) are compared without nonlinearity correction, with nonlinearity correction using estimated fields, and with nonlinearity correction using fields specified by the manufacturer for an ice-water diffusion phantom. The reproducibility is compared between without nonlinearity correction and with nonlinearity correction with the estimated fields for a subject scanned at two positions within the scanner at scanner A. We show that our method removes the need for manufacturer specified SH coefficients and that the method reduces MD reproducibility error in-vivo when the effect of gradient nonlinearities is clearly present.

METHODS

Gradient coil field measurements

Data were acquired across two scanners. Scanner A and scanner B are both 3 Tesla MRI systems on which a phantom is used to estimate the gradient coil fields. The phantom is 24 liters of a synthetic white oil (SpectraSyn 4 polyalphaolefin, ExxonMobil) in a polypropylene carboy with a diameter of 290mm and a height of 500mm [28]. The phantom was placed at scanner isocenter

bioRxiv preprint doi: https://doi.org/10.1101/2020.05.18.102558; this version posted May 20, 2020. The copyright holder for this preprint (which was not certified by peer review) is the author/funder. All rights reserved. No reuse allowed without permission.

and imaged with a dual echo EPI-based field mapping sequence. Images are acquired at two echo times 1ms apart, and the fieldmap is computed from the phase difference of the two images. Four field maps were acquired, one with shim field set to 0.05 mT/m on each axis X, Y, Z plus a final image with gradient coil shim fields set to zero. Each used a 384 mm field of view with 4 mm isotropic voxel size. Total scan time was approximately 5 minutes. Gradient coil fields were estimated by subtracting the zero-shim field map from each coil's respective 0.05 mT/m field map. Field maps were acquired on 40 dates over the course of a year at scanner B while scanner A only one session was acquired with the fieldmapping phantom.

We modeled each coil's field as a sum of solid harmonics [12, 29, 30] to 3rd order, excluding even order terms due to the coils' physical symmetry. These basis functions were fit to the field measurements with robust least squares, using all voxels within a 270 mm diameter sphere at isocenter. The result was an analytically differentiable estimate of the true magnetic field produced by each gradient coil (Figure 1). This fitting procedure was performed on an average field map derived from a series of scans and on the scanner manufacturer's estimate of the coil fields as measured during manufacturing and installation. The series of scans which are averaged are defined for each subject session according to the closest 10 field map sessions in terms of date for scanner B whereas 10 acquisitions were acquired within a single session at scanner A which are averaged.

Estimating achieved b-values and gradient directions

A spatially varying tensor L relates the achieved gradient to the intended gradient [12]:

bioRxiv preprint doi: https://doi.org/10.1101/2020.05.18.102558; this version posted May 20, 2020. The copyright holder for this preprint (which was not certified by peer review) is the author/funder. All rights reserved. No reuse allowed without permission.

$$L = \begin{bmatrix} \frac{\partial B_z^{(x)}}{\partial x} & \frac{\partial B_z^{(y)}}{\partial x} & \frac{\partial B_z^{(z)}}{\partial x} \\ \frac{\partial B_z^{(x)}}{\partial y} & \frac{\partial B_z^{(y)}}{\partial y} & \frac{\partial B_z^{(z)}}{\partial y} \\ \frac{\partial B_z^{(x)}}{\partial z} & \frac{\partial B_z^{(y)}}{\partial z} & \frac{\partial B_z^{(z)}}{\partial z} \end{bmatrix}$$

where $B_z^{(x)}$ is the z component of the magnetic field produced by unit amplitude of a nominal x gradient, and similarly for (y) and (z). This tensor may be computed analytically from the solid harmonic approximation to the measured field, then evaluated at spatial locations of interest. In the common situation where the scanner reports the intended gradient direction and amplitude but the full b-matrix [31-33] is not known, an approximate correction to adjust the intended gradient G for the coil nonlinearity is [18]:

$$G' = LG$$

This estimate of the achieved gradient can then be expressed as the product of an adjusted scalar b-value and a unit vector, $G' = \sqrt{b}g'$. Importantly, this is spatially varying and processing occurs voxelwise, but otherwise this may be used in any desired way for further processing of the diffusion images.

EXPERIMENTS

This section describes the set of analyses which aim to show the accuracy of the estimated fields as well as their impact on resulting DW-MRI metrics in phantom and human data. All DW-MRI are corrected for susceptibility distortion [34] and eddy current distortion [15] using FSL.

bioRxiv preprint doi: https://doi.org/10.1101/2020.05.18.102558; this version posted May 20, 2020. The copyright holder for this preprint (which was not certified by peer review) is the author/funder. All rights reserved. No reuse allowed without permission.

Empirically Estimated Fieldmaps

Gradient non-linearity correction is only viable if we can depend on the estimation to match the true fields. To investigate if the magnitude estimated fieldmaps closely approximate the true fields, we compare them to the fieldmaps specified by the manufacturer on scanner B. For comparison, we take the average fieldmap from the latest 10 oil phantom scans on scanner B and calculate the voxel-wise difference between this and the manufacturer specified fields. To evaluate the stability of the empirical estimations, we report the variance across fields estimated from 40 individual oil phantom scans acquired over time on scanner B. All evaluations on the empirical fields use a spherical mask with a radius of 135mm from isocenter.

Polyvinylpyrrolidone (PVP) phantom

To evaluate the intra-scanner performance of the gradient field nonlinearity correction with the empirical fieldmaps in a controlled environment, we use a 43% Polyvinylpyrrolidone (PVP) aqueous solution in a sealed spherical container (PVP phantom) [35]. The PVP phantom is a large homogeneous material, and estimated metrics are expected to be the same across the entire volume. At scanner B, the phantom was scanned at three positions within the magnet: superior (6cm above isocenter), isocenter, and inferior (6cm below isocenter). At each position twelve directions were acquired at a b-value of 1000 s/mm^2 and twelve more were acquired at 2000 s/mm^2. Susceptibility distortion correction and eddy current distortion correction are applied without movement correction. Resulting signal to noise ratio (SNR) at isocenter, superior position, and inferior position are 89.65, 111.92, and 86.87 respectively. Using all diffusion volumes at each position, FA and MD are calculated without and with gradient nonlinearity correction using the empirically derived fields. We report error without and with nonlinearity correction in terms of reproducibility

bioRxiv preprint doi: https://doi.org/10.1101/2020.05.18.102558; this version posted May 20, 2020. The copyright holder for this preprint (which was not certified by peer review) is the author/funder. All rights reserved. No reuse allowed without permission.

across the three sessions as we would for a human subject. This is done by first registering all non-diffusion volumes to a structural T1 image using a rigid body transform restricted to only use translations. Then we calculate the RMSE between each position and take the average RMSE for each voxel. By acquiring in the three positions in the magnet, we are simulating the worst possible effects of gradient nonlinearity in the z direction.

Human repositioned

To evaluate the inter-scanner performance of the gradient field nonlinearity correction with the empirical fieldmaps in-vivo, we scanned a single subject at scanner A and scanner B. At scanner B, two sessions were acquired of the subject with one session acquired with the subject positioned at isocenter within the magnet and one session acquired with the subject positioned 6cm superior from isocenter. At scanner A, only one session is acquired at isocenter. Each session consisted of twelve gradient directions at a b-value of 1000 s/mm^2 and twelve at a b-value of 2000 s/mm^2. Susceptibility distortion correction and eddy current distortion correction are applied with movement correction for each session. Using all diffusion volumes from each session, FA and MD are calculated without and with gradient nonlinearity correction using the empirically derived fields. For analysis the subject's scans are registered using FSL Flirt [36]. We report error without and with nonlinearity correction in terms of reproducibility error which is in this case the absolute error between MD or FA across scanners.

bioRxiv preprint doi: https://doi.org/10.1101/2020.05.18.102558; this version posted May 20, 2020. The copyright holder for this preprint (which was not certified by peer review) is the author/funder. All rights reserved. No reuse allowed without permission.

RESULTS

Empirically Estimated Fieldmaps

There is small, mostly homogeneous difference between the manufacturer and the measured field produced by the gradient coil. These are shown in Figure 1 in units of mm which are uT/(mT/m). On average the difference at a given voxel is approximately 1 uT/(mT/m) in the x and y gradient fields and 2 uT/(mT/m) in the z gradient field within 135mm of isocenter. The average standard deviation at a given voxel is approximately 4 uT/(mT/m) in the x and y fields and 6 uT/(mT/m) in the z field within 135mm of isocenter.

PVP phantom

We see a large decrease in reproducibility error with nonlinearity correction in both FA and MD across sessions (Figure 2). This is especially evident in superior axial slice in MD. In MD, we see an approximately 66% decrease in the median reproducibility error with nonlinearity correction. In FA, this is approximately 53%. Additionally, because we know the phantom to be an isotropic substance, we report a 25% decrease in the median FA value across all sessions with nonlinearity correction.

Human repositioned

To evaluate the correction's effect on inter-scanner reproducibility in-vivo, we evaluate the absolute error between MD and FA from a single session acquired at scanner A and scanner B of a human subject. First, we look at typical acquisitions which are acquired with the subject positioned at isocenter within the magnet at both scanners. Figure 3 shows the MD without

bioRxiv preprint doi: https://doi.org/10.1101/2020.05.18.102558; this version posted May 20, 2020. The copyright holder for this preprint (which was not certified by peer review) is the author/funder. All rights reserved. No reuse allowed without permission.

nonlinearity correction and the change in MD with nonlinearity correction for both scanners as well as the resulting error in MD without and with nonlinearity correction. The difference between the errors is shown in Figure 4. We find that in the superior axial slices around the edges of the brain where MD is decreased at both scanners with nonlinearity correction, the error is also generally decreased with nonlinearity correction. However, it is not clear in the inferior slices where the MD is increased at both scanners with nonlinearity correction how the correction impacts reproducibility error. Figure 5 shows the median percent change in error for each region as defined by BrainCOLOR and the JHU white matter atlas for FA and MD as well as the distribution of error without and with nonlinearity correction for hierarchical BrainCOLOR regions. While there are some regions which have large relative changes, overall there is not a big shift in error. Across the entire brain volume, the MD reproducibility error increased by approximately 1.8% with nonlinearity correction, and the FA reproducibility error remains approximately unchanged.

Second, we look at a situation in which a typical acquisition is acquired at scanner A and an atypical acquisition is acquired at scanner B where the subject is positioned 6cm superior from isocenter. Figure 6 shows the MD without nonlinearity correction and the change in MD with nonlinearity correction for both scanners as well as the resulting error in MD without and with nonlinearity correction. The difference between the errors is shown in Figure 7. Again, where the correction increases the resulting MD at scanner A in the inferior axial slices, the overall change in error is obscured, but it is clear in the superior slices where MD is increased at scanner B that the correction significantly decreases error. Figure 8 shows the median percent change in error for each region as defined by BrainCOLOR and the JHU white matter atlas for FA and MD as well as

bioRxiv preprint doi: https://doi.org/10.1101/2020.05.18.102558; this version posted May 20, 2020. The copyright holder for this preprint (which was not certified by peer review) is the author/funder. All rights reserved. No reuse allowed without permission.

the distribution of error without and with nonlinearity correction for hierarchical BrainCOLOR regions. While FA is largely unaffected, the MD error is decreased for most regions. Across the entire brain volume, the MD reproducibility error is decreased by approximately 7.1% with nonlinearity correction, and the FA reproducibility error remains approximately unchanged.

DISCUSSION

In comparing the empirically estimated fields to the fields specified by the manufacturer, we find that our approximations are very similar. The largest differences are in the z gradient field which corresponds to the largest variations in all of the estimated fields across 40 oil phantom acquisitions. In this study we use an average fieldmap across 10 acquisitions, but this should not be necessary as the field produced by the gradient coil depends only on the coil geometry and the current flowing in the coils. The current depends on the gain settings which may be changed by the site engineer, but unaltered system need only acquire the fields once for this method. Further study on the stability of the empirical mapping may be necessary. Additionally, further study on the stability of the fit of the spherical harmonics and the need for higher order basis may be necessary.

The PVP phantom experiment shows us that the use of the empirically derived fieldmaps are very effective at reducing intra-scanner reproducibility in a controlled environment when variation is introduced to subject position within the magnet. It also shows that the correction reduces bias in the computed diffusion parameters. In a typical acquisition of in-vivo brain tissue of a single subject, our results show that the correction has very little effect on the resulting MD and FA inter-

bioRxiv preprint doi: https://doi.org/10.1101/2020.05.18.102558; this version posted May 20, 2020. The copyright holder for this preprint (which was not certified by peer review) is the author/funder. All rights reserved. No reuse allowed without permission.

239 scanner reproducibility. However, when the positional variation is introduced, the improvement of
240 MD becomes obvious.

241 In recent work, another approach is proposed for correcting voxel-wise b-value errors. Instead of
242 correcting for gradient nonlinearities in the coil, this method directly estimates a voxel-wise b-
243 value map that is used to correct resulting diffusion metrics [37]. While this method could account
244 for errors that stem from other sources of deviation than just gradient nonlinearities, the model
245 requires an estimation of more parameters and likely it would be best practice to acquire a
246 calibration scan along with every subject acquisition. In comparison to apply the approach
247 proposed in this work, only a single calibration scan is necessary for each system.

248 **CONCLUSION**

249 This work shows that the errors caused by gradient non-linearities is apparent in metrics derived
250 from DW-MRI but can be reduced using the correction outlined by Bammer et al. Using
251 empirically derived fields, we are able to achieve similar results without needing manufacturer
252 specification of the hardware. In both phantom and in-vivo data, error in MD can be significantly
253 reduced by applying this correction. We advocate for the use of gradient non-linearity correction
254 in standard diffusion preprocessing pipelines and provide a simple method for empirically
255 measuring the fields necessary to account for the achieved b-values and b-vectors.

256

bioRxiv preprint doi: https://doi.org/10.1101/2020.05.18.102558; this version posted May 20, 2020. The copyright holder for this preprint (which was not certified by peer review) is the author/funder. All rights reserved. No reuse allowed without permission.

REFERENCES

1. Glover, G.H. and N.J. Pelc, *Method for correcting image distortion due to gradient nonuniformity*. 1986, Google Patents.
2. Michiels, J., et al., *On the problem of geometric distortion in magnetic resonance images for stereotactic neurosurgery.* Magnetic resonance imaging, 1994. **12**(5): p. 749-765.
3. Sumanaweera, T., et al., *Quantifying MRI geometric distortion in tissue.* Magnetic resonance in medicine, 1994. **31**(1): p. 40-47.
4. Langlois, S., et al., *MRI geometric distortion: a simple approach to correcting the effects of non-linear gradient fields.* Journal of Magnetic Resonance Imaging: An Official Journal of the International Society for Magnetic Resonance in Medicine, 1999. **9**(6): p. 821-831.
5. LeBihan, D. and R. Tumer, *Diffusion and perfusion, magnetic resonance imaging, Mozbey Year Book*. 1992, Inc.
6. Conturo, T.E., et al., *Diffusion MRI: precision, accuracy and flow effects.* NMR in Biomedicine, 1995. **8**(7): p. 307-332.
7. Bernstein, M.A. and J.A. Polzin, *Method and system for correcting errors in MR images due to regions of gradient non-uniformity for parametric imaging such as quantitative flow analysis*. 2000, Google Patents.
8. Bammer, R., et al., *Assessment of spatial gradient field distortion in diffusion-weighted imaging.* Proceedings of the International Society for Magnetic Resonance in Medicine , Honolulu, HI, 2002: p. 1172.

bioRxiv preprint doi: https://doi.org/10.1101/2020.05.18.102558; this version posted May 20, 2020. The copyright holder for this preprint (which was not certified by peer review) is the author/funder. All rights reserved. No reuse allowed without permission.

9. Robson, M. *Non-linear gradients on clinical MRI systems introduce systematic errors in ADC and DTI measurements*. in *Proceedings of the 10th Annual Meeting of ISMRM, Honolulu*. 2002.

10. Basser, P.J. and C. Pierpaoli, *Microstructural and physiological features of tissues elucidated by quantitative-diffusion-tensor MRI.* Journal of Magnetic Resonance Imaging, 2011. **213**(2): p. 560-570.

11. Frank, L.R., *Anisotropy in high angular resolution diffusion-weighted MRI.* Magnetic Resonance in Medicine: An Official Journal of the International Society for Magnetic Resonance in Medicine, 2001. **45**(6): p. 935-939.

12. Bammer, R., et al., *Analysis and generalized correction of the effect of spatial gradient field distortions in diffusion-weighted imaging.* Magnetic Resonance in Medicine: An Official Journal of the International Society for Magnetic Resonance in Medicine, 2003. **50**(3): p. 560-569.

13. Setsompop, K., et al., *Pushing the limits of in vivo diffusion MRI for the Human Connectome Project.* Neuroimage, 2013. **80**: p. 220-233.

14. Malyarenko, D.I., et al., *Demonstration of nonlinearity bias in the measurement of the apparent diffusion coefficient in multicenter trials.* J Magnetic resonance in medicine, 2016. **75**(3): p. 1312-1323.

15. Andersson, J.L. and S.N. Sotiropoulos, *An integrated approach to correction for off-resonance effects and subject movement in diffusion MR imaging.* Neuroimage, 2016. **125**: p. 1063-1078.

16. McNab, J.A., et al., *The Human Connectome Project and beyond: initial applications of 300 mT/m gradients.* Neuroimage, 2013. **80**: p. 234-245.

bioRxiv preprint doi: https://doi.org/10.1101/2020.05.18.102558; this version posted May 20, 2020. The copyright holder for this preprint (which was not certified by peer review) is the author/funder. All rights reserved. No reuse allowed without permission.

17. Mesri, H.Y., et al., *The adverse effect of gradient nonlinearities on diffusion MRI: From voxels to group studies.* NeuroImage, 2019: p. 116127.

18. Tan, E.T., et al., *Improved correction for gradient nonlinearity effects in diffusion-weighted imaging.* Journal of Magnetic Resonance Imaging, 2013. **38**(2): p. 448-453.

19. Newitt, D.C., et al., *Gradient nonlinearity correction to improve apparent diffusion coefficient accuracy and standardization in the american college of radiology imaging network 6698 breast cancer trial.* Journal of Magnetic Resonance Imaging, 2015. **42**(4): p. 908-919.

20. Malyarenko, D.I., B.D. Ross, and T.L. Chenevert, *Analysis and correction of gradient nonlinearity bias in apparent diffusion coefficient measurements.* Magnetic resonance in medicine, 2014. **71**(3): p. 1312-1323.

21. Malyarenko, D.I. and T.L. Chenevert, *Practical estimate of gradient nonlinearity for implementation of apparent diffusion coefficient bias correction.* Journal of Magnetic Resonance Imaging, 2014. **40**(6): p. 1487-1495.

22. Sotiropoulos, S.N., et al., *Advances in diffusion MRI acquisition and processing in the Human Connectome Project.* Neuroimage, 2013. **80**: p. 125-143.

23. Glasser, M.F., et al., *The minimal preprocessing pipelines for the Human Connectome Project.* Neuroimage, 2013. **80**: p. 105-124.

24. Janke, A., et al., *Use of spherical harmonic deconvolution methods to compensate for nonlinear gradient effects on MRI images.* Magnetic Resonance in Medicine: An Official Journal of the International Society for Magnetic Resonance in Medicine, 2004. **52**(1): p. 115-122.

bioRxiv preprint doi: https://doi.org/10.1101/2020.05.18.102558; this version posted May 20, 2020. The copyright holder for this preprint (which was not certified by peer review) is the author/funder. All rights reserved. No reuse allowed without permission.

25. Doran, S.J., et al., *A complete distortion correction for MR images: I. Gradient warp correction.* Physics in Medicine & Biology, 2005. **50**(7): p. 1343.

26. Tao, S., et al., *Integrated image reconstruction and gradient nonlinearity correction.* Magnetic resonance in medicine, 2015. **74**(4): p. 1019-1031.

27. Rogers, B.P., et al. *Phantom-based field maps for gradient nonlinearity correction in diffusion imaging*. in *Medical Imaging 2018: Physics of Medical Imaging*. 2018. International Society for Optics and Photonics.

28. Rogers, B.P., et al. *Stability of gradient field corrections for quantitative diffusion MRI*. in *Medical Imaging 2017: Physics of Medical Imaging*. 2017. International Society for Optics and Photonics.

29. Tough, R.J. and A.J. Stone, *Properties of the regular and irregular solid harmonics.* Journal Of Physics A: Mathematical General, 1977. **10**(8): p. 1261.

30. Caola, M., *Solid harmonics and their addition theorems.* Journal of Physics A: Mathematical General, 1978. **11**(2): p. L23.

31. Mattiello, J., P.J. Basser, and D. Le Bihan, *The b matrix in diffusion tensor echo-planar imaging.* Magnetic Resonance in Medicine, 1997. **37**(2): p. 292-300.

32. Mattiello, J., P.J. Basser, and D. LeBihan, *Analytical expressions for the b matrix in NMR diffusion imaging and spectroscopy.* Journal of magnetic resonance, Series A, 1994. **108**(2): p. 131-141.

33. Alger, J.R., *The diffusion tensor imaging toolbox.* Journal of Neuroscience, 2012. **32**(22): p. 7418-7428.

bioRxiv preprint doi: https://doi.org/10.1101/2020.05.18.102558; this version posted May 20, 2020. The copyright holder for this preprint (which was not certified by peer review) is the author/funder. All rights reserved. No reuse allowed without permission.

343 34. Andersson, J.L., S. Skare, and J. Ashburner, *How to correct susceptibility distortions in*
344 *spin-echo echo-planar images: application to diffusion tensor imaging.* Neuroimage, 2003.
345 **20**(2): p. 870-888.
346 35. Pierpaoli, C., et al. *Polyvinylpyrrolidone (PVP) water solutions as isotropic phantoms for*
347 *diffusion MRI studies*. in *Proc Intl Soc Magn Reson Med*. 2009.
348 36. Jenkinson, M., et al., *Improved optimization for the robust and accurate linear registration*
349 *and motion correction of brain images.* Neuroimage, 2002. **17**(2): p. 825-841.
350 37. Lee, Y., et al., *A comprehensive approach for correcting voxel-wise b-value errors in*
351 *diffusion MRI.* 2019.

352

353
354

bioRxiv preprint doi: https://doi.org/10.1101/2020.05.18.102558; this version posted May 20, 2020. The copyright holder for this preprint (which was not certified by peer review) is the author/funder. All rights reserved. No reuse allowed without permission.

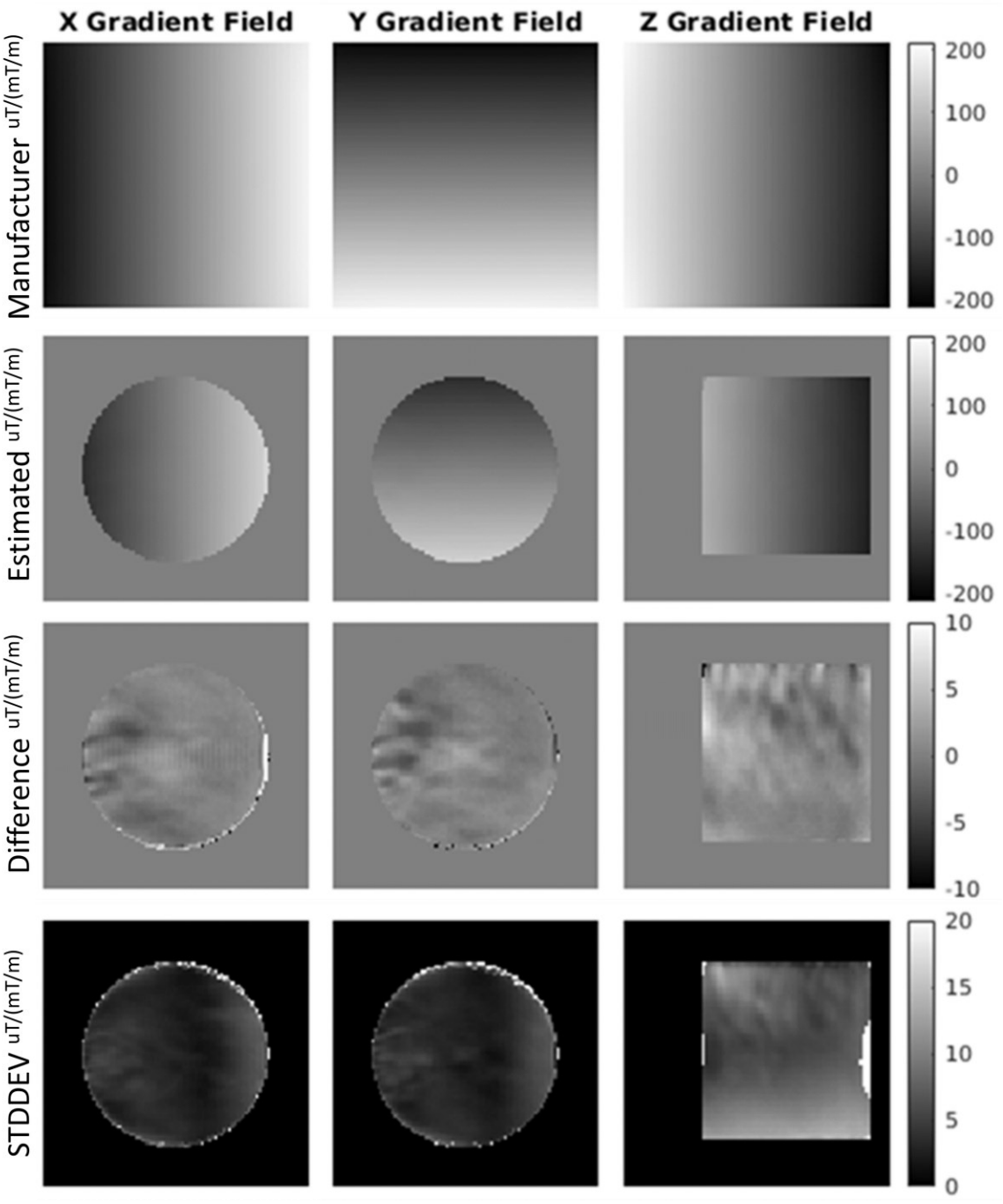

Figure 1: Here we show the manufacturer specified fields (top), the averaged empirically estimated (directly measured) fields (middle-top), the difference between these (middle-bottom), and the standard deviation in the empirically estimated fields across time (bottom) in units of uT/(mT/m). The field of view is 384mm by 384mm, and a mask is applied to the fields according the usable regions within the oil phantom (135mm radius from isocenter). The x and y gradient fields are shown as an axial slices at isocenter (192mm), and the z gradient field is shown as a sagittal slice at isocenter (192mm).

bioRxiv preprint doi: https://doi.org/10.1101/2020.05.18.102558; this version posted May 20, 2020. The copyright holder for this preprint (which was not certified by peer review) is the author/funder. All rights reserved. No reuse allowed without permission.

356

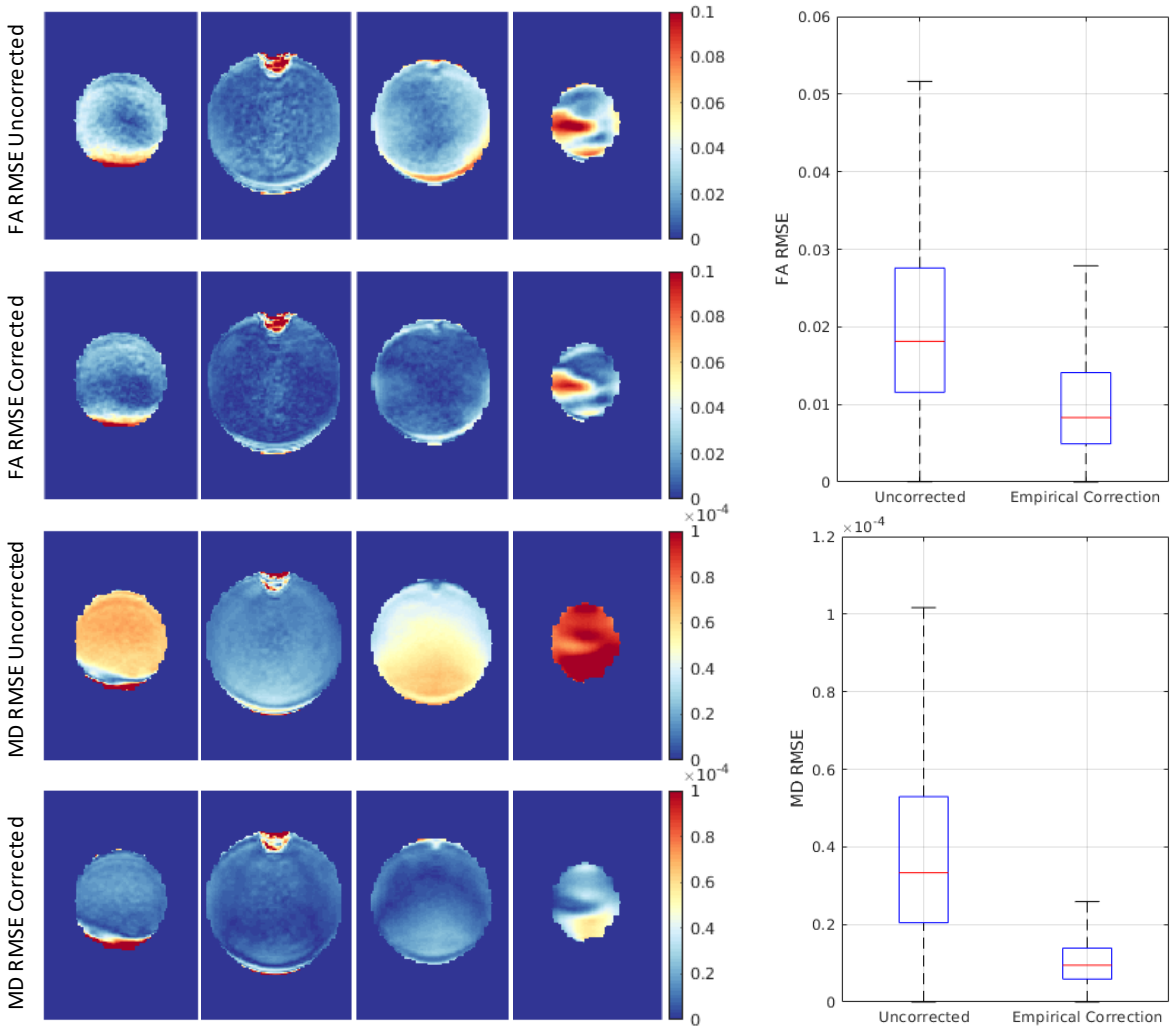

Figure 2: The FA and MD reproducibility in four axial slices (inferior left to superior right) in the PVP phantom without and with nonlinearity correction is applied using the empirically estimated fields (left). The dimensions of an axial slice are 256mm by 170mm (1mm by 2mm voxel resolution). The median, 25th percentile, and 75th percentile are shown in the boxplots (right). The large reduction in error can be seen across the volume.

357

358

bioRxiv preprint doi: https://doi.org/10.1101/2020.05.18.102558; this version posted May 20, 2020. The copyright holder for this preprint (which was not certified by peer review) is the author/funder. All rights reserved. No reuse allowed without permission.

359

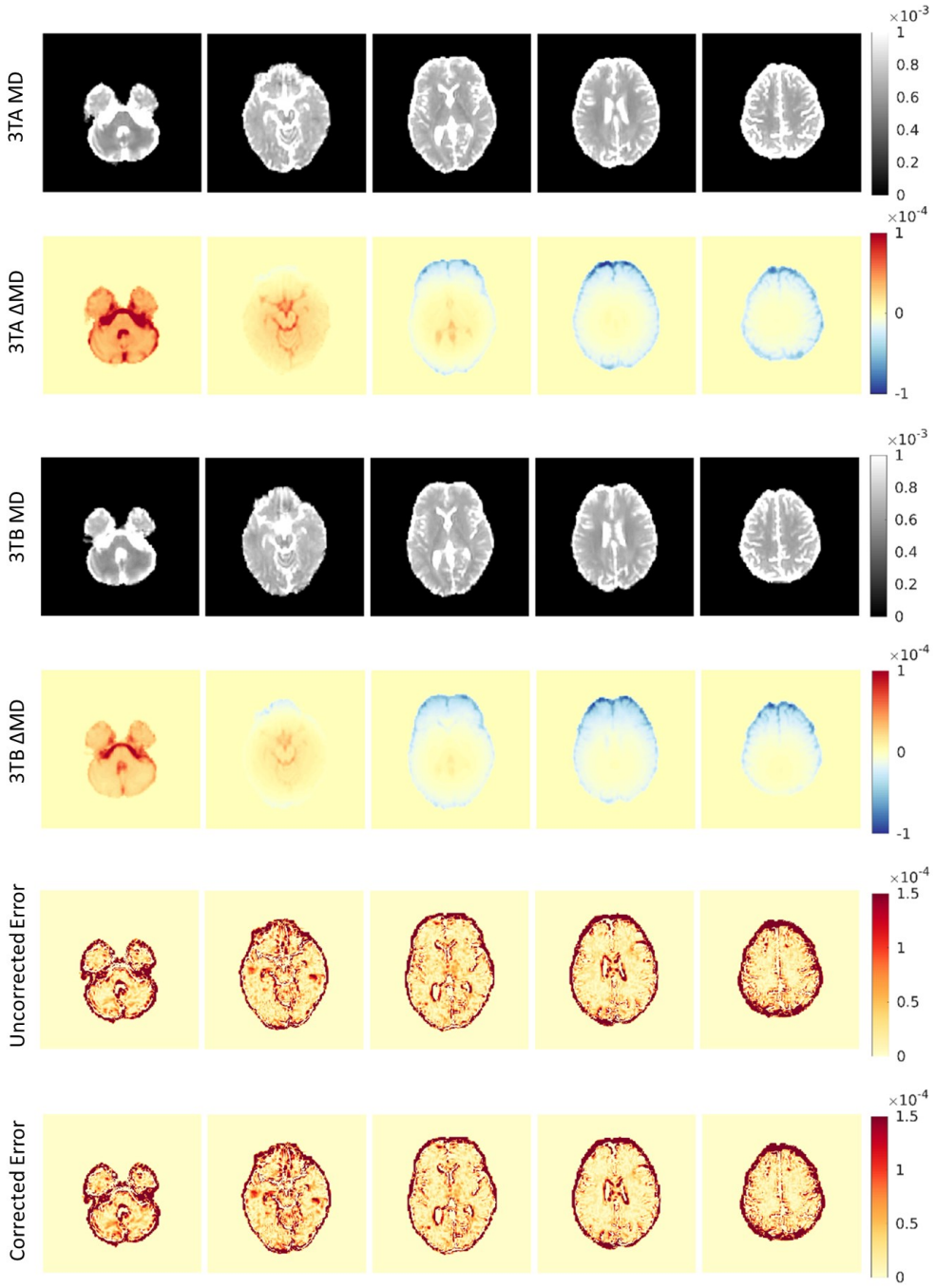

Figure 3: For the DW-MRI acquisitions at scanner A (3TA) and scanner B (3TB) acquired at isocenter as is typical, we show MD at scanner A, the change in MD with nonlinearity correction at scanner A, the MD at scanner B, the change in MD with nonlinearity correction at scanner B, the absolute reproducibility error without nonlinearity correction, and the absolute reproducibility with nonlinearity correction from top row to bottom row for five axial slices. A mask is used to exclude CSF regions in the error.

bioRxiv preprint doi: https://doi.org/10.1101/2020.05.18.102558; this version posted May 20, 2020. The copyright holder for this preprint (which was not certified by peer review) is the author/funder. All rights reserved. No reuse allowed without permission.

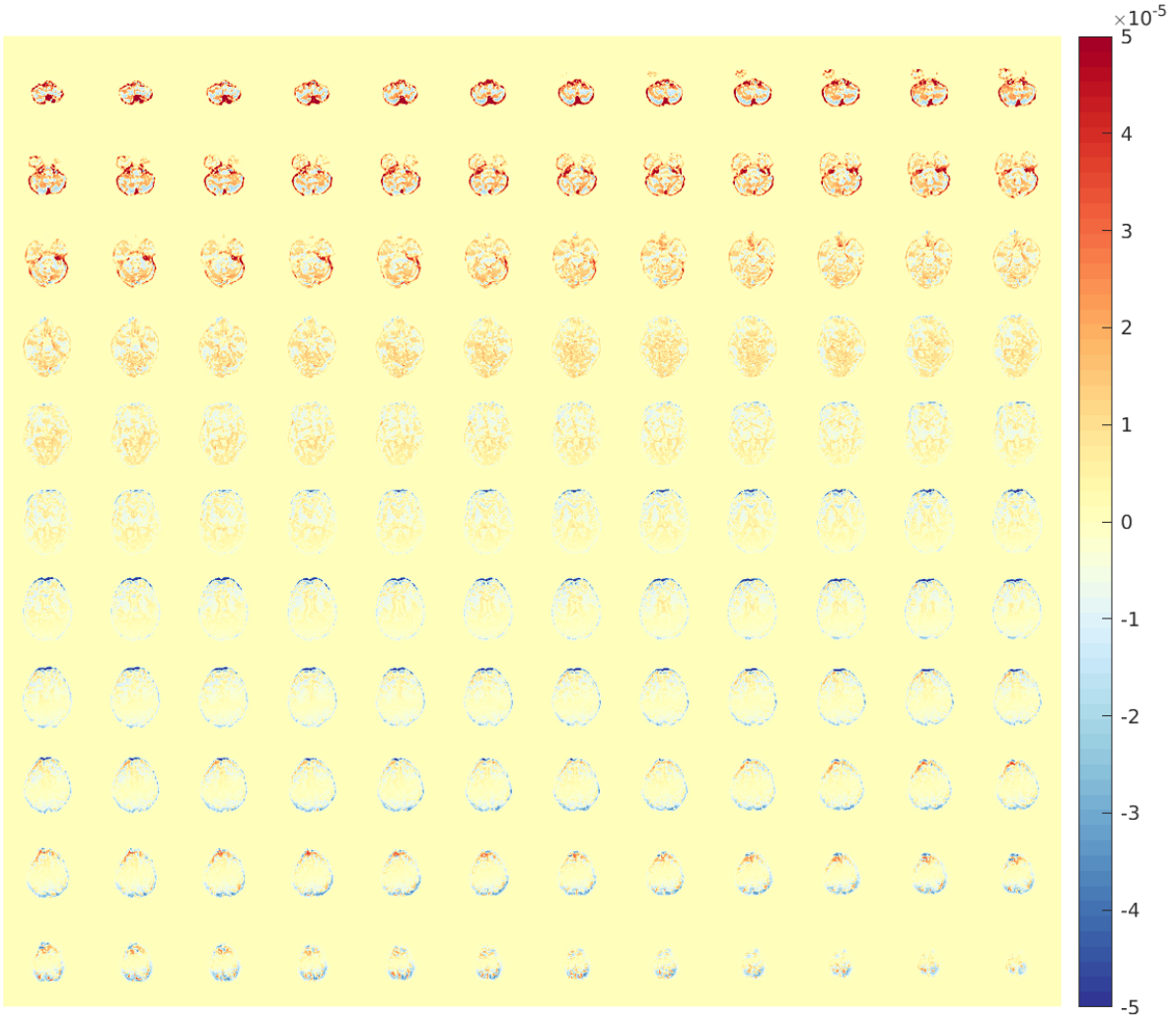

Figure 4: For the DW-MRI acquisitions at scanner A and scanner B acquired at isocenter, we show the change in reproducibility error (uncorrected error subtracted from corrected error) for every axial slice. Positive values indicate an increase in error with nonlinearity correction, and negative values indicate a decrease in error. A mask is used to exclude CSF regions in the error.

bioRxiv preprint doi: https://doi.org/10.1101/2020.05.18.102558; this version posted May 20, 2020. The copyright holder for this preprint (which was not certified by peer review) is the author/funder. All rights reserved. No reuse allowed without permission.

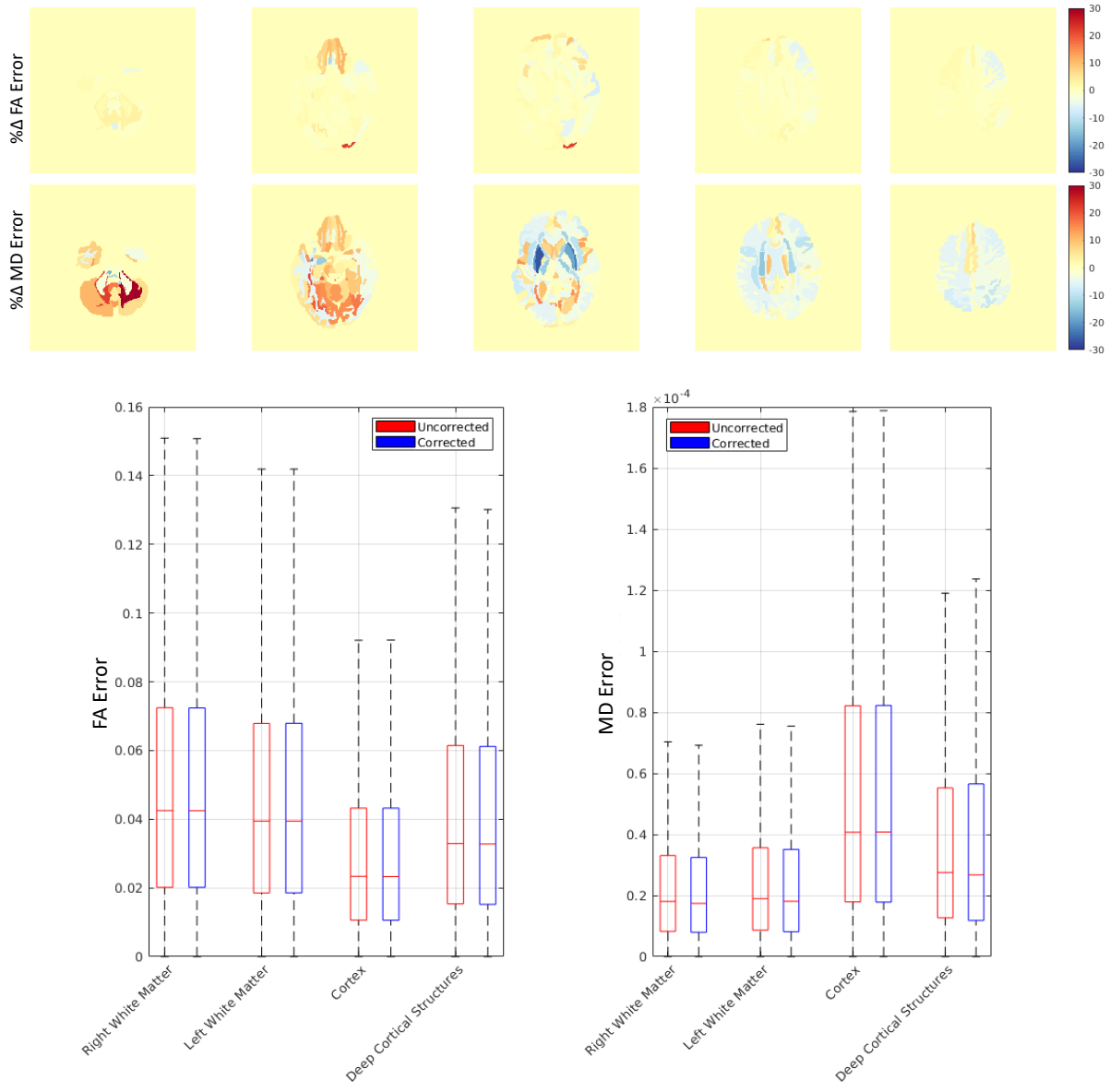

Figure 5: For the DW-MRI acquisitions at scanner A and scanner B acquired at isocenter, we show the percent change in median FA error by region according to the BrainCOLOR and JHU white matter atlas and the same for MD in the top two rows, and we show the absolute reproducibility error in four hierarchical regions for FA and MD the bottom row.

363

bioRxiv preprint doi: https://doi.org/10.1101/2020.05.18.102558; this version posted May 20, 2020. The copyright holder for this preprint (which was not certified by peer review) is the author/funder. All rights reserved. No reuse allowed without permission.

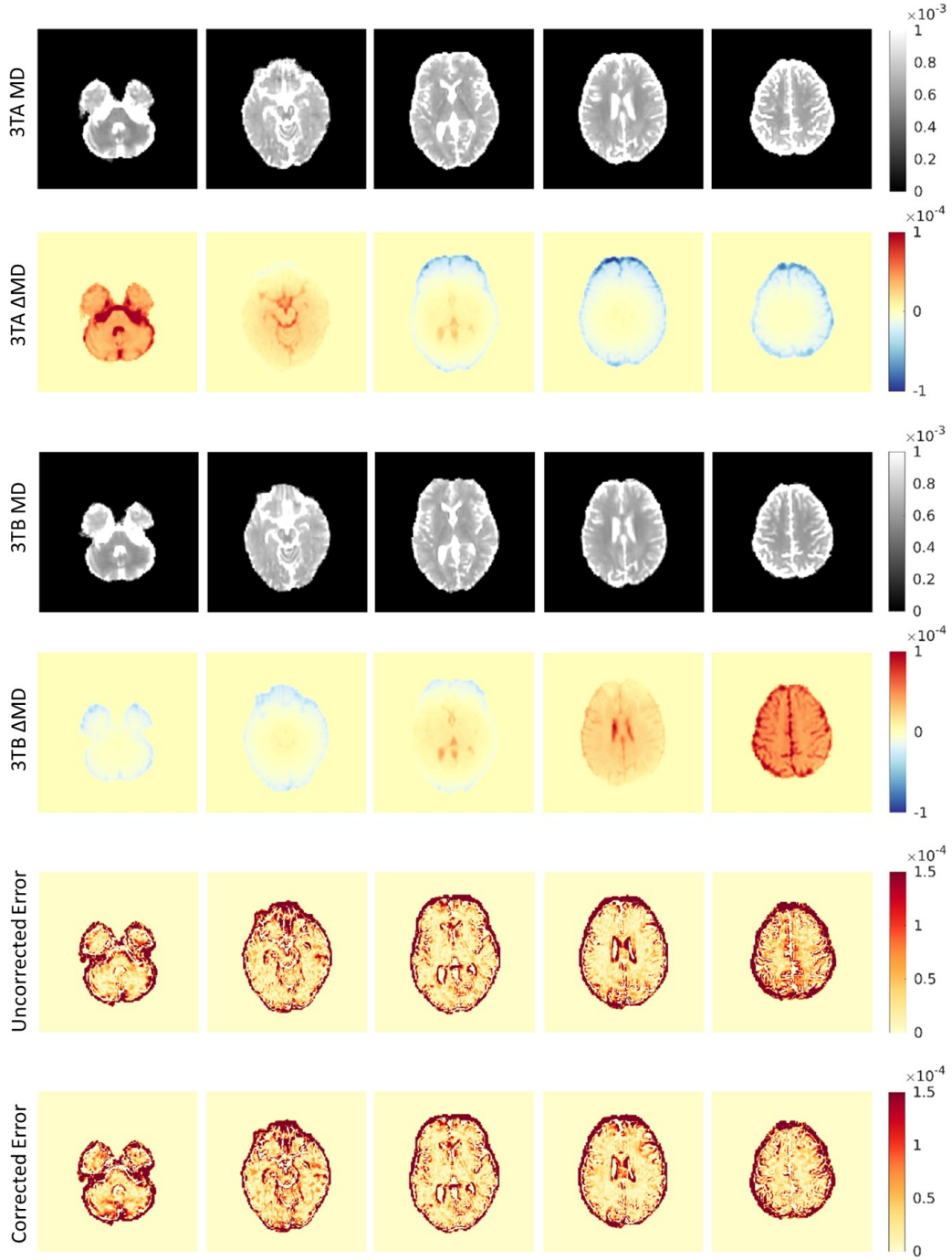

Figure 6: For the DW-MRI acquisitions at scanner A (3TA) acquired at isocenter and scanner B (3TB) acquired 6cm superior to isocenter, we show MD at scanner A, the change in MD with nonlinearity correction at scanner A, the MD at scanner B, the change in MD with nonlinearity correction at scanner B, the absolute reproducibility error without nonlinearity correction, and the absolute reproducibility with nonlinearity correction from top row to bottom row for five axial slices. A mask is used to exclude CSF regions in the error.

bioRxiv preprint doi: https://doi.org/10.1101/2020.05.18.102558; this version posted May 20, 2020. The copyright holder for this preprint (which was not certified by peer review) is the author/funder. All rights reserved. No reuse allowed without permission.

365

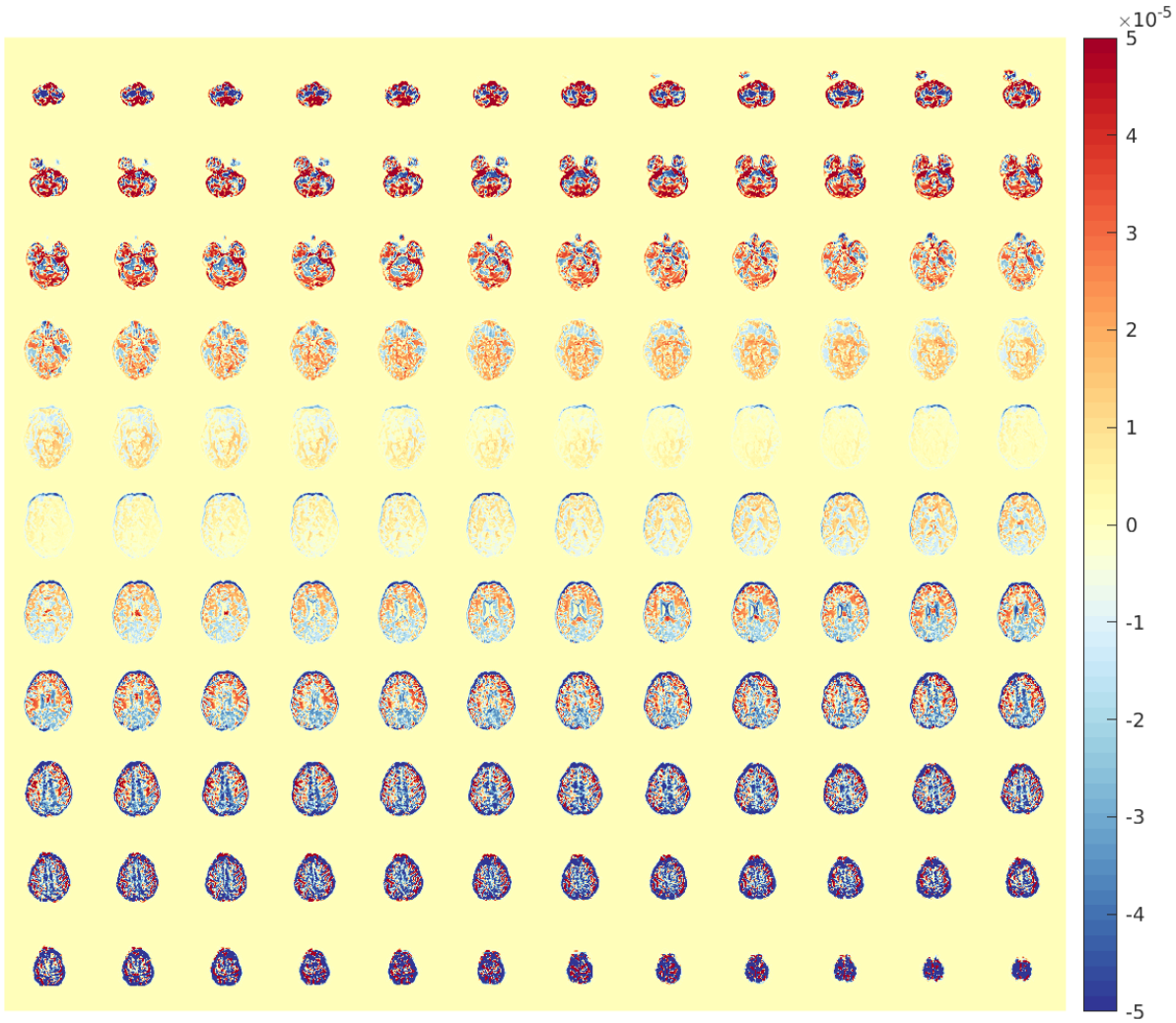

Figure 7: For the DW-MRI acquisitions at scanner A acquired at isocenter and scanner B acquired 6cm superior to isocenter, we show the change in reproducibility error (uncorrected error subtracted from corrected error) for every axial slice. Positive values indicate an increase in error with nonlinearity correction, and negative values indicate a decrease in error. A mask is used to exclude CSF regions in the error.

366

367

bioRxiv preprint doi: https://doi.org/10.1101/2020.05.18.102558; this version posted May 20, 2020. The copyright holder for this preprint (which was not certified by peer review) is the author/funder. All rights reserved. No reuse allowed without permission.

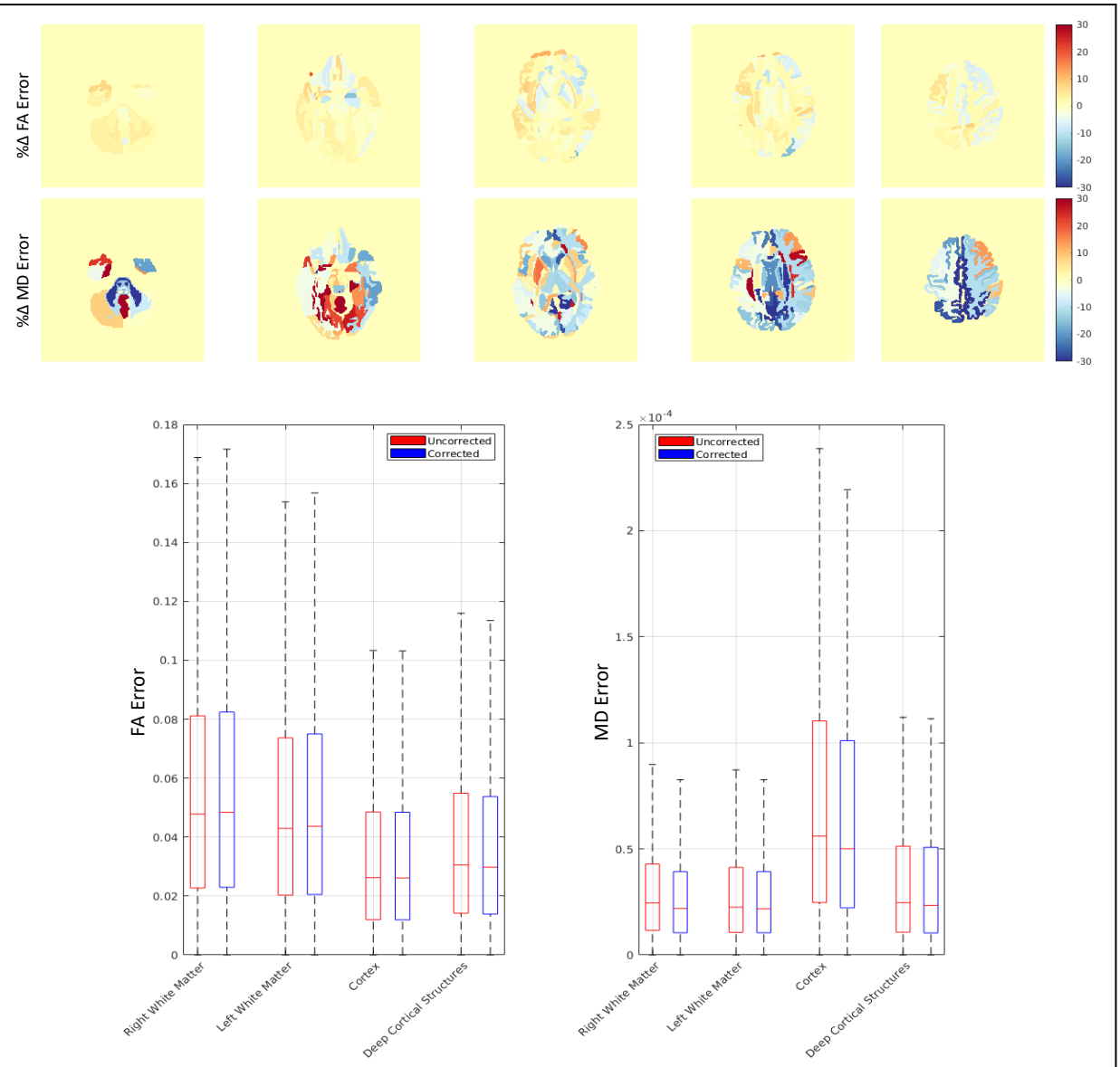

Figure 8: For the DW-MRI acquisitions at scanner A acquired at isocenter and scanner B acquired 6cm superior to isocenter, we show the percent change in median FA error by region according to the BrainCOLOR and JHU white matter atlas and the same for MD in the top two rows, and we show the absolute reproducibility error in four hierarchical regions for FA and MD the bottom row.

368